Title: Alzheimer's disease clinical variants show distinct regional patterns of neurofibrillary tangle accumulation

Cathrine Petersen[1], Amber L Nolan[1], Elisa de Paula França Resende[1], Alexander Ehrenberg[1], Salvatore Spina[1], Bruce L. Miller[1], William Seeley[1], Zachary Miller[1], Lea T. Grinberg[1]

[1] Memory and Aging Center, Weill Institute for Neurosciences, University of California, San Francisco

Send correspondence to:
Lea Tenenholz Grinberg, MD, PhD, Associate Professor in Residence
Memory and Aging Center, Department of Neurology
Sandler Neurosciences Center, Box 1207
675 Nelson Rising Lane, Room 211B
San Francisco, CA 94158
E-mail: lea.grinberg@ucsf.edu

This study was supported by K24AG053435 and institutional grants P50AG023501, P01AG019724.

The authors have no duality or conflicts of interest to declare.

ABSTRACT

Background: Neurofibrillary tangle (NFT) pathology in Alzheimer's disease (AD) follows a stereotypic progression well-characterized by Braak staging. However, some AD cases show deviations from the Braak staging scheme. In this study, we tested the hypothesis that these variations in the regional distribution of tau pathology are linked to heterogeneity in the clinical phenotypes of AD.

Methods: We included a clinicopathological cohort of ninety-four AD cases enriched for atypical clinical presentations. Subjects underwent apolipoprotein E (APOE) genotyping and neuropsychological testing. Main cognitive domains (executive, visuospatial, language, and memory function) were assessed using an established composite z-score. We assessed NFT density and distribution from thioflavin S fluorescent microscopy throughout four neocortical and two hippocampal regions. A mathematical algorithm classifying AD cases into typical, hippocampal sparing (HpSp), and limbic predominant (LP) subtypes based on regional NFT burden was compared to unbiased hierarchical clustering for cases with Braak stage > IV.

Results: Patients diagnosed with logopenic primary progressive aphasia showed significantly higher NFT density in the superior temporal gyrus relative to patients diagnosed with Alzheimer-type dementia ($p = 0.0091$), while patients with corticobasal syndrome showed significantly higher NFT density in the primary motor cortex ($p = 0.0205$). Hierarchical clustering identified three discrete clusters of patients characterized respectively by low overall NFT burden ($n = 18$), high overall burden ($n = 30$), and cortical-predominant burden ($n = 24$). A regionally specific effect was observed for visuospatial ability; higher NFT density in the angular gyrus ($\beta = -0.0921$, $p = 0.0099$) and in the CA1 sector of the hippocampus ($\beta = -0.0735$, $p = 0.0380$) was significantly associated with more severe visuospatial dysfunction, modulated by age of death.

Conclusions: Our results suggest domain-specific functional consequences of regional NFT accumulation. In particular, we observed focal aggregation of NFT density in clinically relevant regions among different clinical AD variants. Continued work to map the regionally specific clinical consequences of tau accumulation presents an opportunity to increase understanding of disease mechanisms underlying atypical clinical manifestations.

INTRODUCTION

Pathologically proven Alzheimer's disease (AD) can present clinically with a range of cognitive symptoms beyond the classic progressive amnestic-predominant decline. These atypical clinical manifestations include corticobasal syndrome, logopenic variant primary progressive aphasia, posterior cortical atrophy, as well as dysexecutive syndromes resembling behavioral variant frontotemporal dementia [1].

Younger age at onset has been associated with greater non-amnestic deficits in AD relative to late-onset (≥ 65 years of age) AD [3]. Further, co-occurring neurodegenerative pathologies have been posited to contribute to the variability in clinical phenotypes of AD patients. For instance, the co-occurrence of Lewy body pathology has been suggested to accelerate cognitive decline and clinical heterogeneity [1, 2].

In AD, the microtubule-associated protein tau aggregates form neurofibrillary tangles (NFTs), one of the hallmark structural lesions of AD. Tau pathology is highly deleterious to synaptic function and is closely linked to cognitive decline [4, 5]. The Braak and Braak staging scheme of neurofibrillary changes characterizes the stereotypic progression of regional deposition of NFT pathology from the brainstem and transentorhinal cortex, to the hippocampus, and finally to the association and primary cortices [6]. However, some AD cases show deviations from the Braak staging scheme. Mapping the regional distribution of tau NFT pathology in these cases may further our understanding of the pathological underpinnings of clinical variants of AD.

Murray et al. suggested in 2011 that two neuropathologically distinct atypical subtypes of AD exist: hippocampal sparing AD (HpSp) and limbic predominant AD (LP), each with characteristic sets of clinical attributes distinct from typical AD. Specifically, patients with HpSp were younger and predominantly male, whereas patients with LP were older, with a higher proportion of women. HpSp cases were found to include a significantly higher proportion of atypical clinical syndromes [3, 7].

In vivo neuroimaging studies using the tau positron emission tomography tracer ^{18}F-AV1451 have shown relevant regional differences in tau uptake among clinical variants of AD [8].

Ossenkoppele et al. reported that patients with posterior cortical atrophy showed outsized ^{18}F-AV1451 patterns specific to the clinically relevant posterior brain regions and three out of five patients with logopenic variant primary progressive aphasia showed asymmetric higher left hemisphere ^{18}F-AV1451 retention. In addition, regionally relevant ^{18}F-AV1451 uptake was associated with domain-specific neuropsychological tests in memory (medial temporal lobes), visuospatial function (occipital, right temporoparietal cortex), and language (left temporoparietal cortex) [8].

Here we extend these findings in a large post-mortem clinicopathological sample to clarify the clinical relevance of regional tau pathology to multiple clinical variants of AD and domain-specific cognitive decline. We hypothesized that: (i) unique regional distributions of NFT would correlate with different clinical variants of AD; and (ii) that NFT density in different brain regions would correlate with worse performance on cognitive tests of associated domains. To investigate this hypothesis, we systematically mapped the average NFT density throughout selected representative neocortical and hippocampal sections in a cohort of patients enriched for atypical presentations of AD. We investigated regional trends in NFT accumulation and their association with clinical and demographic variables.

METHODS

This study was approved by the UCSF Ethical Committee and all the participants or their legal representatives signed a written informed consent that was obtained according to the Declaration of Helsinki and its further amendments.

Participants

All participants were recruited from the clinicopathological cohort of the Memory and Aging Center at the University of California, San Francisco (UCSF). Each individual underwent in-depth neurological history, examination and comprehensive neuropsychological and functional assessment including the Clinical Dementia Rating at least once. All these participants underwent an extensive dementia-oriented postmortem assessment covering dementia-related regions of interest on the left hemisphere unless upon gross pathology the right was noted to be more atrophic. Neuropathological diagnosis followed currently accepted guidelines [9-13].

Subtyping for FTLD-TDP and FTLD-tau followed the current "harmonized" nomenclature [14, 15].

We included ninety-four participants with a primary neuropathologic diagnosis of AD neuropathological change based on consensus criteria with varying levels of severity, and with or without argyrophilic grain disease (AGD) and age-related tau astrogliopathy [16]. All participants lacked presence of other cortical neuropathological changes such as TDP-43 proteinopathies, alpha-synuclein pathologies, other well-defined tauopathies or cerebrovascular contributing lesions. This sample is enriched for atypical clinical variants of AD.

Clinical history

Prior to autopsy, participants were evaluated longitudinally at the Memory and Aging Center at UCSF through an in-depth neurological history, examination, and extensive neuropsychological assessment. The clinical diagnosis was determined by chart review based on published criteria for the diagnoses: Alzheimer-type dementia [17-19], corticobasal degeneration syndrome [20], logopenic primary progressive aphasia [21], posterior cortical atrophy syndrome [22, 23], behavioral variant frontotemporal dementia [24, 25], and mild cognitive impairment (MCI) [26, 27].

Final diagnosis for cases with atypical features including prominent language, visuospatial, motor, and behavioral deficits were determined by consensus between two investigators. One patient presented with rapid cognitive decline, hyper-solomnence, parkinsonism, and ataxia and did not meet criteria for any of the mentioned variants of AD. This patient's syndrome will be referred to as "Other," and will be excluded from group comparisons of diagnoses that require more than one case per diagnosis. A diagnosis of MCI required a Clinical Dementia Rating (CDR) score of 0.5, and all the cognitively healthy participants had a CDR score of zero in the post-mortem evaluation using an informant.

In addition to clinical diagnosis, demographic and genetic features were collected for all patients with available data. Age of symptoms onset, age at death, disease duration, sex, and years of education were included for analysis. Genotyping of the apolipoprotein E (APOE) allele was

performed using a TaqMan Allelic Discrimination Assay on an ABI 7900HT Fast Real-Time polymerase chain reaction system (Applied Biosystems).

The neuropsychological assessment included a test battery that covered four major cognitive domains: executive function [design fluency, letter fluency, Stroop test (correct naming), digital backwards, and Trail making B (number of correct lines in one minute)], language ability (Boston Naming test [28], fluency of animals in one minute, Peabody Picture Vocabulary Test [29], and Information subtest of Verbal IQ from the Wechsler scale), visuospatial ability (modified Rey figure, number location of the Visual Object and Space Perception battery, and block design of the Wechsler Adult Intelligence Scale -III), and memory [California Verbal Learning Test (delayed recall, sum of the learning trials, and recognition accounting for false positives), and modified Rey figure delayed recall]. Performance for each of these four cognitive domains (executive, language, visuospatial, and memory function) was assessed through a pre-defined calculated composite score averaging the z-scores from the collected neuropsychological raw data [30]. These z-scores are calculated relative to normative data from a cohort of cognitively healthy older adults [31]. These composite scores are used in lieu of specific neuropsychological test performance in order to enhance sensitivity to domain dysfunction and reduce the dimensionality of cognitive assessment data.

Neuropathological assessment

Using thioflavin-S fluorescent microscopy, quantitative measures of NFT densities were assessed with a ZEISS Axio Scan.Z1 fluorescent slide scanner microscope. The regions examined for each subject included four neocortical regions: the middle frontal gyrus, superior temporal gyrus, primary motor cortex, and angular gyrus; and two hippocampal regions: the CA1 and subiculum. These regions were chosen as representative association cortices and hippocampal regions across a range of functional domains and classical vulnerability to AD pathology.

The neuroanatomical sampling design and procedures for thioflavin S fluorescent microscopy used in this study were informed by techniques developed originally by Terry and colleagues [32]. Briefly, 8μm-thick paraffin-embedded sections were stained using thioflavin-S, and regions

of interest were imaged. Three 500 μm^2 areas were sampled at random from each region, and quantitative NFT counts were averaged across these three areas to produce a density score.

Thioflavin-S identifies NFT pathology as well as β-amyloid neuritic plaques (Figure 1). NFT pathology was distinguished from β-amyloid pathology based on the distinct morphological differences between the aggregates. NFT pathology is distinguished by flame-shaped or globose morphology of fibrous neuronal aggregates. NFT counts included intracellular and extracellular tangles.

Statistical analysis

A Kruskal-Wallis test with post hoc pairwise Mann-Whitney U tests was used to evaluate the differences in cognitive domain composite z-scores and regional NFT densities among the clinical diagnostic groups. To account for multiple testing, the false discovery rate was set at <0.05. For these analyses, MCI and cognitively normal patients are treated as one diagnostic group, and only diagnostic groups with more than one patient are considered.

Multivariate linear regression was used to evaluate the relationships between regional NFT density and demographic covariates. Additionally, multivariate linear regression was used to evaluate the relationships between regional and overall NFT density and domain-specific cognitive function, accounting for clinical covariates.

Principal component analysis was used to analyze the relationships between NFT density in different brain regions. We abided by Kaiser's criterion, to retain only those factors that have eigenvalues > 1 [33], and Cattell's criterion, which uses a scree plot of eigenvalues and retains all factors in the sharp descent prior to the inflection point [34]. Factor meaningfulness and interpretability were taken into consideration, along with contribution to total variance.

We applied an unbiased clustering analysis to define neuropathological classifications based on the regional NFT density throughout all brain regions examined. We validated Ward's method of hierarchical clustering against other clustering methodologies, such as k-means clustering, based on three internal validation criteria: connectivity, silhouette width, and the Dunn index [35]. The

validation was done in R, using the Cluster Validation Package clValid [36]. In order to select the optimal number of clusters, we used the elbow method for a plot of within groups sum of squares and the number of clusters [37]. The resulting clusters were contrasted in terms of demographics and neuropsychological composite scores using a Kruskal-Wallis test with *post hoc* Mann-Whitney U-test comparisons. To account for multiple testing, the false discovery rate was again set at <0.05. A Chi Square test was used to compare the proportion of males and of APOE ε4 allele carriers across the groups.

Subjects were classified as HpSp, LP, and typical subtypes, based on the relative density of NFTs in the hippocampus and three association cortices. The detailed algorithm methods have been previously described [3]. Briefly, to qualify as HpSp, a case must pass three requirements. First, the ratio of the average hippocampal NFT to the average cortical NFT must be less than the 25th percentile of all cases. Second, all three of the hippocampal NFT densities must be less than the median values. Third, at least two of the cortical NFT measures must be greater than or equal to the median values. To qualify as LP, a case must pass the converse three requirements. If a case is meets criteria for neither HpSp or LP, it is classified as the typical AD subtype. Both the k-means clustering and algorithmic partitioning was limited to cases with Braak stage > IV to limit the effect of disease progression on group membership.

Statistical analyses were performed using R Statistical Software (version 3.4.4; R Foundation for Statistical Computing, Vienna, Austria).

RESULTS

Demographics

Of the ninety-four participants, fifty-six (59.6%) were male. The mean (SD) age of symptoms onset was 60.8 (10.5) years, the mean (SD) age of death was 71.2 (10.9) years, and the mean (SD) disease duration was 10.4 (3.7) years. The mean (SD) educational attainment was 15.9 (3.3) years. In 44.2% of the participants, at least one copy of the APOE ε4 allele was present. This cohort predominantly features severe disease stages. Seventy-six participants (80.9%) were evaluated at Braak stage VI for neurofibrillary changes. Eighty-three participants (88.3%) were evaluated to have frequent neuritic plaque pathology by CERAD criteria.

Fifty-two participants (55.3%) were diagnosed with typical Alzheimer-type dementia, whereas thirty-one (33.0%) were diagnosed with an atypical clinical variant: eight participants were diagnosed with corticobasal syndrome, eight with logopenic variant primary progressive aphasia, seven with behavioral variant frontotemporal dementia, seven with posterior cortical atrophy, and one with an unspecified clinical syndrome. In addition, seven cases met criteria for MCI and four were cognitively healthy at death. Demographic and clinical characteristics for each diagnostic group are presented in Table 1.

Domain-specific cognitive deficits differ among AD clinical variants

Predictably, patients with logopenic variant primary progressive aphasia showed significantly more severe impairment on language tasks than patients diagnosed with typical Alzheimer-type dementia ($p = 0.0021$), while patients with posterior cortical atrophy performed significantly worse on visuospatial tasks relative to patients diagnosed with typical Alzheimer-type dementia ($p = 0.0038$). The cohort of MCI and cognitively normal patients performed significantly better relative to all other diagnostic groups ($n > 1$) on executive, language, and visuospatial tasks. For memory tasks, the only significant difference was between typical Alzheimer-type dementia and the MCI and cognitively normal cohort ($p = 0.0243$). Summary statistics are presented in Table 2A.

Distinct regional patterns of NFT accumulation characterize AD clinical variants

The focal regions of prominent NFT accumulation differ among AD clinical variants. Figure 1B shows the mean regional NFT density for each diagnostic group ($n > 1$). Summary statistics are presented in Table 2. Notably, the patients with logopenic primary progressive aphasia not only had significantly increased cortical tau pathology relative to MCI and cognitively normal patients, but also showed significantly higher NFT density in the superior temporal gyrus relative to patients diagnosed with Alzheimer-type dementia ($p = 0.0091$). Patients with corticobasal syndrome showed significantly higher NFT density in the primary motor cortex relative to patients diagnosed with Alzheimer-type dementia ($p = 0.0205$).

NFT density in the CA1 region of the hippocampus did not significantly differ between any diagnostic groups. Patients with Alzheimer-type dementia or with corticobasal syndrome showed significantly higher NFT density relative to the MCI and cognitively normal group in four out of five regions: the middle frontal gyrus, superior temporal gyrus, primary motor cortex, angular gyrus, and subiculum. Patients with logopenic variant primary progressive aphasia or with posterior cortical atrophy showed significantly higher NFT density relative to the MCI and cognitively normal group in just the cortical regions: the middle frontal gyrus, superior temporal gyrus, primary motor cortex, and angular gyrus. Finally, the patients with behavioral variant frontotemporal dementia showed significantly higher NFT density relative to the MCI and cognitively normal group in the middle frontal gyrus, superior temporal gyrus, and angular gyrus.

The regional axes of variation in tau pathology are clinically relevant

Principal component analysis of NFT regional density data retained two components, together accounting for 78.22% of the variance in regional NFT density and revealing co-localization of NFT accumulation along two axes: cortical and hippocampal (Figure 2A). This dimensionality reduction appears to have some usefulness in discriminating patients with certain atypical clinical variants – namely corticobasal syndrome, logopenic variant primary progressive aphasia, and posterior cortical atrophy – from those with Alzheimer-type dementia, MCI, and healthy controls, whereas the patients with behavioral variant frontotemporal dementia are not clearly discriminable (Figure 2B).

Multivariate linear regression correcting for demographic covariates sex, disease duration, age of death, years of education, and APOE ε4 allele presence showed a significant inverse correlation of cortical NFT burden (an average of the densities in the middle frontal gyrus, superior temporal gyrus, primary motor cortex, and angular gyrus) with age of death ($\beta = -0.9486$, $p < 0.0001$). Hippocampal NFT burden (an average of the densities in the CA1 and subiculum sectors of the hippocampus) showed a significant positive association with disease duration ($\beta = 1.8713$, $p = 0.0004$). NFT burden was found to be significantly higher among women in both cortical regions and hippocampal regions ($\beta = 8.2835$, $p = 0.0017$; $\beta = 9.4098$, $p = 0.0111$), correcting for

covariates. There was no significant relationship between the regional NFT burden of APOE ε4 allele carriers and non-carriers.

Using Ward's method of hierarchical clustering, we identified three unbiased discrete clusters of patients with varying regional NFT burden (Figure 3A). Clinical and demographic data was not included in the clustering algorithm, which was based solely on regional NFT pathology densities. The resulting clusters appear to be characterized by low overall NFT burden (n = 18), high overall burden (n = 30), and cortical-predominant burden (n = 24). These results are compared to the algorithmic partition into HpSp (n = 6), LP (n = 6), and Typical (n = 60) subtypes (Figure 3B). The clinical associations of the k-means clusters and algorithmic subtypes are summarized in Table 3. Both the k-means clustering and algorithmic partitioning was limited to cases with Braak stage > IV to limit the effect of disease progression on group membership [3].

Associations of regional NFT accumulation with neuropsychological performance

Increased cortical NFT burden significantly correlated with more severe cognitive dysfunction in after correcting for demographic covariates and the time elapsed between the neuropsychological tests and death, for all four domains: executive function ($\beta = -0.0449$, $p = 0.0033$), language ability ($\beta = -0.1147$, $p = 0.0201$), visuospatial ability ($\beta = -0.1103$, $p = 0.0379$), and memory ($\beta = -0.0583$, $p = 0.0055$). In contrast, increased hippocampal NFT burden correlated with more severe cognitive dysfunction in just two domains: executive function ($\beta = -0.0215$, $p = 0.0470$) and memory ($\beta = -0.0380$, $p = 0.0053$).

The collinearity of NFT density among the five assessed regions makes it difficult to parse region-specific effects on relevant cognitive domains. Even so, a strong regionally specific effect was observed for visuospatial ability; higher NFT density in the angular gyrus ($\beta = -0.0921$, $p = 0.0099$) and in the CA1 sector of the hippocampus ($\beta = -0.0735$, $p = 0.0380$) was significantly associated with more severe dysfunction as measured by the visuospatial domain composite z-score, albeit significantly modulated by age of death.

DISCUSSION

This study mapped NFT burden throughout six cortical and hippocampal sections to examine associations between tau pathology and clinical characteristics in a well-characterized clinicopathological series of participants with a heterogeneous clinical presentation.

We found that regional tau pathology shows a marked deviance from typical AD progression in atypical clinical variants of AD. We observed significantly lower cortical NFT burden with increasing age, similar to previous reports [38]. Both cortical and hippocampal NFT burden differed significantly by sex. These results are consistent with, and expand on past findings from neuroimaging, post-mortem, animal, and cerebrospinal fluid studies suggesting that regional tau aggregation is closely linked to the clinical manifestations of AD. We found no significant difference in regional NFT density between APOE ε4 allele carriers and non-carriers, likely due to the high proportion of Braak stage VI cases in this sample. Braak stage VI has been shown to be overrepresented among APOE ε4 allele carriers, relative to non-carriers [39].

The cases of most interest in our analysis were those diagnosed with a syndrome outside of Alzheimer-type dementia during life. Visual inspection and formal comparisons indicated that tau selectively aggregated in regions that are clinically affected. Predictably, subjects diagnosed with MCI or normal cognitive function showed significantly low overall density. Patients with Alzheimer-type dementia and with corticobasal syndrome showed significantly higher NFT density relative to the MCI and cognitively normal group in five out of six regions: the middle frontal gyrus, superior temporal gyrus, primary motor cortex, angular gyrus, and subiculum. Patients with logopenic variant primary progressive aphasia or with posterior cortical atrophy showed significantly higher NFT density relative to the MCI and cognitively normal group in just the cortical regions: the middle frontal gyrus, superior temporal gyrus, primary motor cortex, and angular gyrus. Finally, the patients with behavioral variant frontotemporal dementia showed significantly higher NFT density relative to the MCI and cognitively normal group in the middle frontal gyrus, superior temporal gyrus, and angular gyrus. Though the subiculum appears prominently affected in these patients, one patient with a clinical diagnosis of behavioral variant frontotemporal dementia had only negligible tau pathology in the subiculum, creating a large variation which precludes statistical significance.

Overall, these regions are implicated in a variety of cognitive functions, and it appears that generally, atypical clinical variants may show higher cortical tau accumulation than patients with Alzheimer-type dementia. NFT density in the CA1 region of the hippocampus did not significantly differ between any diagnostic groups. This region seems conspicuously absent as a significant pinpoint for the amnestic-predominant Alzheimer-type dementia. It is possible that the CA1 region reaches a saturation-point early in the progression of AD-type tau pathology regardless of the clinical variant.

Our findings are novel in showing through pathological comparisons that certain regions differ significantly in NFT burden between specific atypical clinical variants and Alzheimer-type dementia. Patients with logopenic primary progressive aphasia showed significantly higher NFT density in the superior temporal gyrus relative to patients diagnosed with Alzheimer-type dementia. Logopenic variant primary progressive aphasia is clinically characterized by predominant impaired single-word retrieval and impaired repetition [21]. The superior temporal gyrus distinguished patients with logopenic variant primary progressive aphasia from patients with Alzheimer-type dementia, in line with previous work showing temporoparietal tau accumulation stereotypic to this variant [40].

In addition, patients with corticobasal syndrome showed significantly higher NFT density in the primary motor cortex relative to patients diagnosed with Alzheimer-type dementia. Corticobasal syndrome features usually features symptom onset of motor deficits such as stiffness, often followed by language impairment such as word-finding difficulties [20].

Discrete patterns of NFT accumulation may contribute to the variation in clinical presentation of AD. In order to parse these contributions, we used unbiased hierarchical clustering to identify patterns within groups of patients based on regional accumulation of NFT. Observationally, the three clusters appear to be characterized by low overall NFT burden, high overall burden, and cortical-predominant burden, respectively. These clusters were contrasted to the subtype classifications of HpSp, LP, and typical AD defined by Murray et al. (Table 3), which are algorithmically more highly discretized, but sacrifice cohesion within each subtype [3].

Overall, the hierarchical partitioning of clusters showed high relevance to clinical characteristics, despite the exclusion of clinical and demographic data from the clustering algorithm, which was based solely on regional NFT pathology densities.

HpSp, LP, and typical AD subtypes differ significantly only along disease duration. However, the lack of significant results may derive from the small sample sizes of HpSp (n = 6) and LP (n = 6) subtypes. Clinical characteristics appear to follow the same trends described by Murray et al [3]. Manually defined algorithms rely on assumptions about what can be considered "typical," and which differences warrant distinction. This algorithm, specifically, constructs the categories, HpSP and LP, along expectations of which cases should fit an atypical profile. In doing so, it achieves highly dichotomized pathologic profiles in each "atypical" group but masks the spectrum of pathologic presentation. These results suggest that the ratio between hippocampal and cortical NFT density may not be a primary driver of clinical heterogeneity and that clinically relevant pathologic groupings may be more complex than previously suggested.

The strength of hierarchical clustering is its unbiased approach to grouping similar patients based on their pathologic profiles; in doing so, it acknowledges the full spectrum of pathologic differences. These results, along with the significant correlation of overall NFT density to all four cognitive domains, suggest that overall NFT burden, which is conflated in the algorithm subtypes, may be the primary driver of cognitive function. However, the characteristic patterns within our k-means partitioning implicates specific regional accumulation of NFT as a contributor to the clinical presentation of AD, which may be contingent on differential regional vulnerability to tau pathology. In lieu of a more rigorous definition of clusters in a larger sample, these results were used as exploratory data analysis to guide our inquiries into specific regional associations of NFT density to clinical characteristics.

Higher NFT density in the angular gyrus and CA1 was significantly associated with more severe visuospatial dysfunction. These inquiries were predicated on well-documented functional associations of each specific region. The angular gyrus is implicated in spatial cognition, and the CA1 has more recently been implicated in spatial encoding in addition to its well-documented role in memory [41-43]. These associations suggest domain-specific functional consequences of

regional NFT accumulation. Further investigation is needed to assess the underlying mechanisms connecting NFT to regional selective vulnerability. Evaluating these kinds of regional relationships between atypical presentations of AD and β-amyloid distribution would be an interesting area for further study, however NFT pathology has been shown to be a better predictor of clinical phenotype and subsequent atrophy [44-46].

This study has several strengths. We were well-equipped to explore clinical correlates of neuronal tau pathology in a sample of patients seen by dementia specialists with extensive experience characterizing atypical presentations of neurodegenerative disease. Our raw neuropsychological test data was comprehensive, allowing for well-informed assessments of cognitive dysfunction based on composite scores. Clustering analysis was validated against other methods in accordance with three well-documented indices of internal validation, assessing the compactness, connectedness, and separation of the cluster partitions.

Our insight into specific atypical clinical syndromes was limited by a low number of subjects within each diagnosis. Further studies may benefit from a focus on a single clinical variant, such as logopenic variant primary progressive aphasia. Further, these clinical diagnoses reflect symptoms at onset; therefore, it is possible that the clinical relevance of tau pathology measured post-mortem is not captured in the clinical diagnosis. In addition, a larger sample would allow for higher-resolution insight into the regional patterns by which NFT accumulates. Clustering analyses are accompanied and complicated by ongoing research into the optimization of methods and best practices. It is generally accepted that to prescribe a single technique to every situation or dataset is ineffective, and it has been indicated that pragmatic approaches which compare multiple methods for effectiveness do fairly well. The choice of number of groups is similarly fraught and centered in an understanding that despite the prevalence of formalized criteria, there is no completely satisfactory or universal method [47]. Further, for both the hierarchical clustering method as well as the algorithmic subtypes, the resultant partitioning is sample-dependent; cutoff values for inclusion in each group are contingent on the collective sample data. For these reasons, validation and more rigorous definition of the identified clusters in a separate and/or larger sample would prove particularly insightful.

Additionally, it is notable that the patients evaluated at the Memory and Aging Center at the University of California, San Francisco are homogenous with regard to certain demographic and pathologic features. First, our sample was predominantly Braak stage VI, making it difficult to assess the full impact of Braak stage on these analyses, as well as the potential differential patterns of atypical NFT accumulation across classically defined Braak stages. Second, our sample was predominantly white (89.4%) with a high level of education. It would be valuable to validate these results in a separate cohort with a more representative spread of education, race, and tau burden.

In summary, this study highlights the clinical relevance of regional patterns of NFT accumulation in a subset of AD patients. Our results suggest domain-specific functional consequences of regional NFT accumulation. In particular, we observed focal aggregation of NFT density in clinically relevant regions among different clinical AD variants. Further, the angular gyrus and CA1 subfield of the hippocampus with correlated specifically with visuospatial ability. Continued work to map the regionally specific clinical consequences of tau accumulation presents an opportunity to increase understanding of disease mechanisms underlying atypical clinical manifestations.

Figures

Table 1. Demographic characteristics according to diagnostic group.

Clinical diagnosis	n	Proportion male	Mean age of onset (SD)	Mean age of death (SD)	Mean disease duration (SD)	Years of education (SD)	Proportion APOE ε4 carriers
Alzheimer-type dementia	52	0.67	62.63 (10.53)	73.21 (10.83)	10.43 (3.56)	15.86 (3.91)	0.54
Corticobasal syndrome	8	0.38	57.88 (10.05)	67.88 (9.49)	10.00 (3.66)	16.14 (3.08)	0.25
Logopenic variant primary progressive aphasia	8	0.38	56.13 (5.41)	66.63 (6.19)	10.50 (2.00)	15.63 (2.13)	0.29
Behavioral variant frontotemporal dementia	7	0.86	51.57 (6.55)	64.43 (7.18)	12.86 (5.34)	15.80 (2.68)	0.43
Posterior cortical atrophy	7	0.14	53.14 (2.73)	63.14 (3.80)	10.00 (3.61)	15.86 (1.46)	0.17
Other	1	1.00	58.00 (-)	66.00 (-)	8.00 (-)	16.00 (-)	1.00
Mild cognitive impairment	7	0.43	73.43 (7.44)	82.57 (4.86)	9.14 (4.81)	16.43 (2.94)	0.29
Cognitively normal	4	1.00	-	86.75 (12.82)	-	15.25 (1.50)	0.50
Total	94	0.60	60.80 (10.46)	71.99 (10.87)	10.43 (3.70)	15.88 (3.27)	0.44

Figure 1. Mean regional NFT densities according to diagnostic group (n > 1).

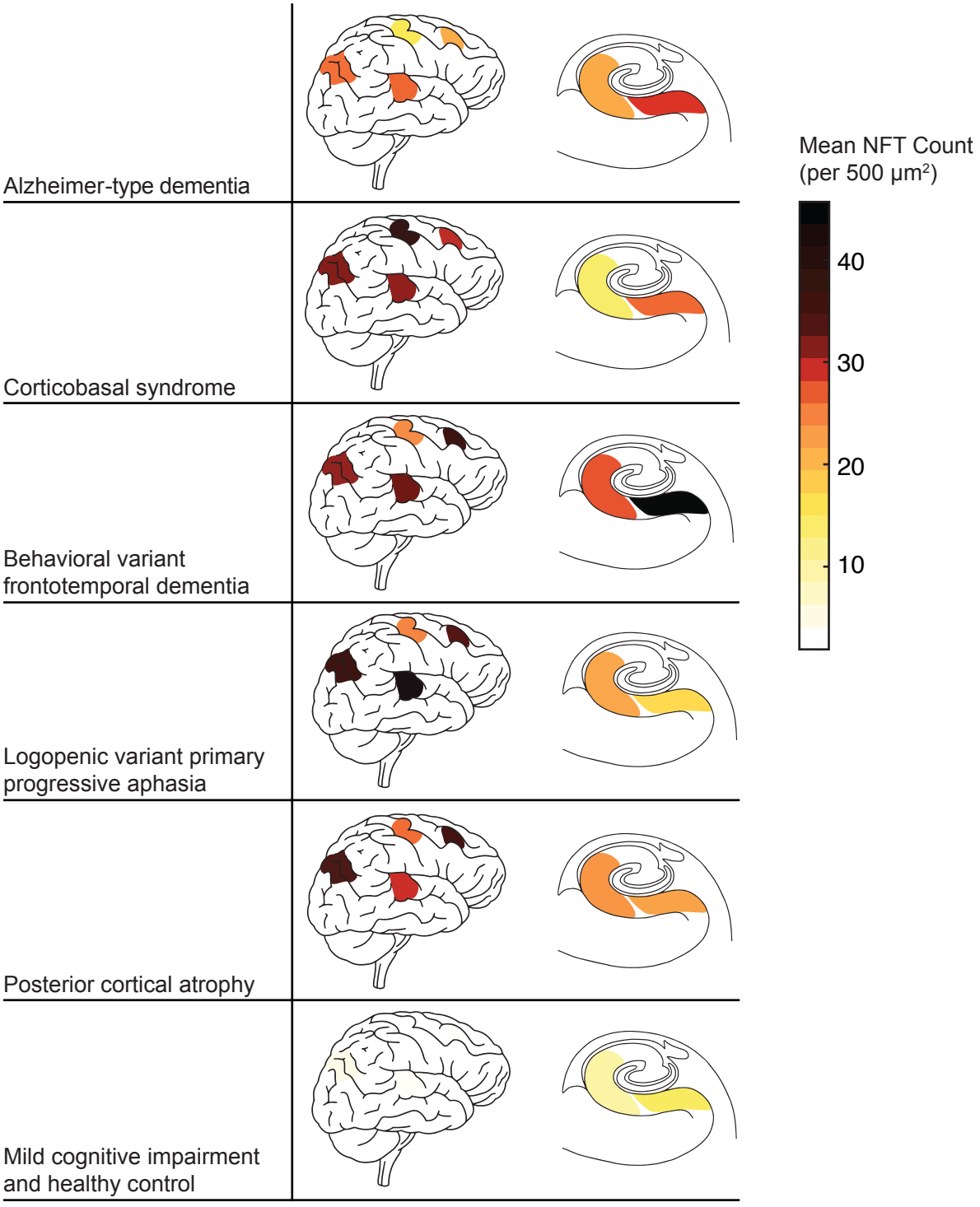

Table 2. Summary statistics for (**A**) cognitive domain composite z-scores and (**B**) regional NFT densities according to diagnostic group. Differences between groups (n > 1) were assessed using a Kruskal-Wallis test with *post hoc* Mann-Whitney U-test pairwise comparisons. The false discovery rate (FDR) was set at < 0.05.

Pairwise comparisons of each diagnostic group (n > 1) with the MCI and cognitively normal group:

* FDR-corrected p < 0.05

** FDR-corrected p < 0.01

*** FDR-corrected p < 0.001

Pairwise comparisons of each atypical diagnostic group (n > 1) with the Alzheimer-type dementia group:

† FDR-corrected p < 0.05

†† FDR-corrected p < 0.01

A

		Mean composite z-score (SD)				
Clinical diagnosis	n	Executive function	Language ability	Visuospatial ability	Memory function	Mean CDR-SOB (SD)
Alzheimer-type dementia	52	-3.01 (1.35)***	-3.58 (1.93)**	-5.16 (3.31)**	-4.01 (1.44)*	9.36 (5.08)***
Corticobasal syndrome	8	-3.26 (0.72)**	-6.05 (3.54)*	-6.62 (5.05)*	-3.90 (1.74)	8.31 (5.82)**
Logopenic variant primary progressive aphasia	8	-3.83 (0.35)**	-7.59 (3.19)**††	-6.96 (3.51)**	-4.41 (1.53)	12.63 (3.42)**
Behavioral variant frontotemporal dementia	7	-3.72 (1.26)**	-4.85 (2.34)*	-5.30 (2.97)*	-4.13 (2.21)	10.80 (6.35)*
Posterior cortical atrophy	7	-3.20 (0.71)**	-7.46 (5.52)**	-10.12 (2.24)**††	-4.50 (1.54)	12.64 (5.59)**
Other	1	-4.00 (-)	-3.26 (-)	-1.74 (-)	-4.02 (-)	15.00 (-)
MCI and cognitively normal	11	-0.53 (0.75)	-1.35 (1.12)	-0.41 (1.07)	-1.24 (1.93)	1.09 (1.16)
Total	94	-2.88 (1.43)	-4.33 (3.14)	-5.33 (3.88)	-3.88 (1.70)	8.95 (5.69)

B

		Mean NFT density per 500 μm² (SD)					
Clinical diagnosis	n	Middle frontal gyrus	Superior temporal gyrus	Primary motor cortex	Angular gyrus	CA1	Subiculum
Alzheimer-type dementia	52	20.05 (17.86)*	24.76 (19.13)**	14.60 (14.11)*	24.33 (16.70)**	20.31 (15.98)	27.13 (26.03)*
Corticobasal syndrome	8	29.04 (17.95)**	29.96 (13.43)**	33.58 (17.38)**†	33.21 (12.44)**	14.08 (5.88)	26.08 (7.27)*
Logopenic variant primary progressive aphasia	8	32.96 (11.88)**	42.63 (8.43)**††	24.83 (11.55)**	36.21 (14.97)**	21.92 (11.64)	16.79 (10.78)
Behavioral variant frontotemporal dementia	7	30.67 (16.97)*	27.62 (16.23)*	21.67 (23.06)	26.62 (16.00)**	23.43 (16.52)	38.24 (33.50)
Posterior cortical atrophy	7	35.24 (15.54)**	29.24 (9.59)**	26.11 (10.77)*	33.89 (9.60)**	23.52 (16.37)	22.33 (11.35)
Other	1	4.00 (-)	6.33 (-)	2.33 (-)	4.67 (-)	6.67 (-)	8.00 (-)
MCI and cognitively normal	11	3.27 (3.50)	2.76 (3.93)	3.94 (4.74)	3.64 (5.45)	7.70 (6.76)	8.70 (9.58)
Total	94	21.70 (18.05)	24.49 (18.33)	17.10 (15.85)	24.24 (17.01)	18.75 (14.68)	24.26 (23.10)

Figure 2. Results of Principal Component Analysis. Principal component 1 accounted for 59.42% of the variance in regional density, and principal component 2 accounted for 18.81% of the variance. **A.** Variable factor loadings for retained components of regional NFT density principal component analysis. **B.** Individual patient loadings for each principal component by diagnosis. Atypical clinical variants are highlighted.

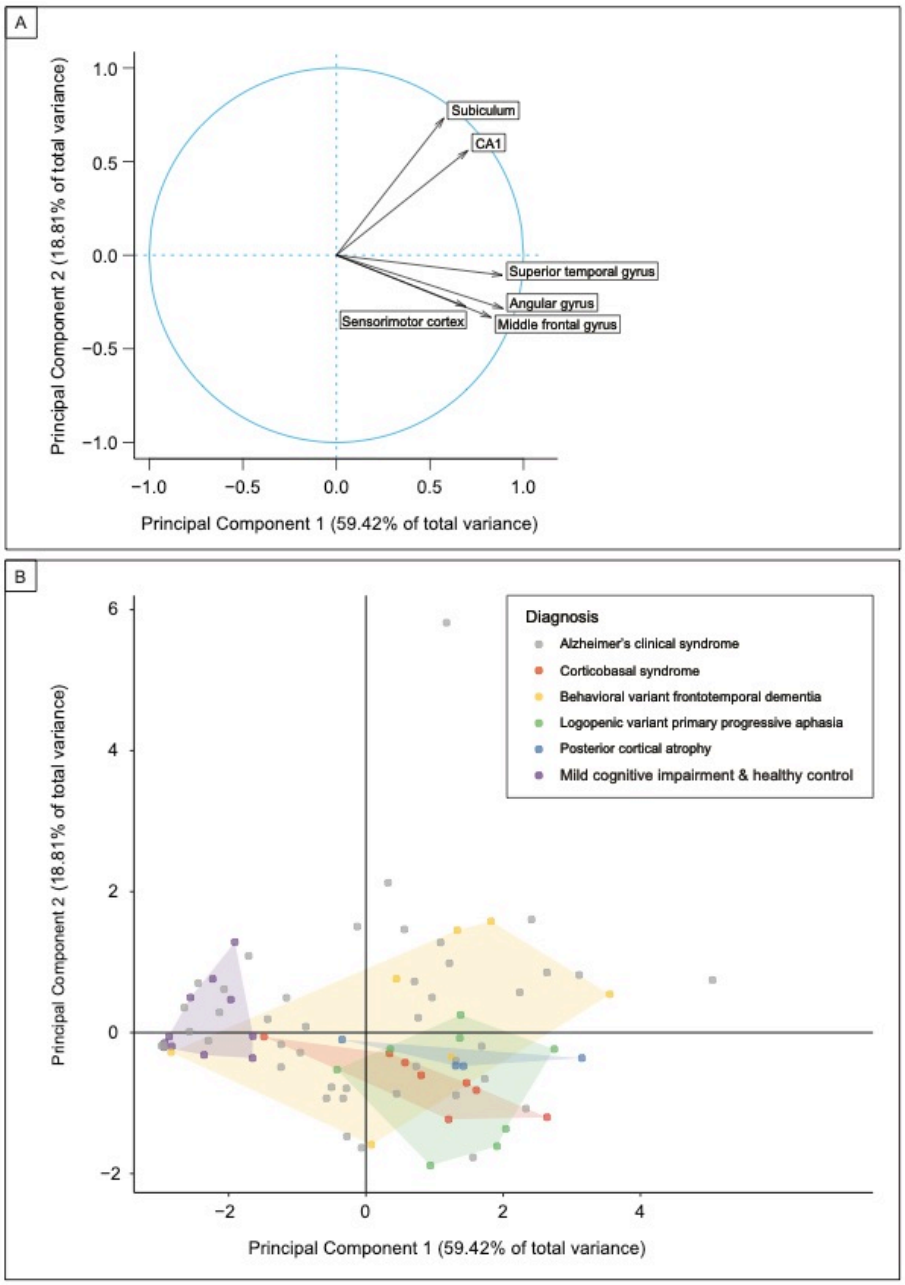

Figure 3. Patient clusters based on regional NFT densities. **A.** Partition using k-means clustering. **B.** Partition using previously defined algorithm [3].

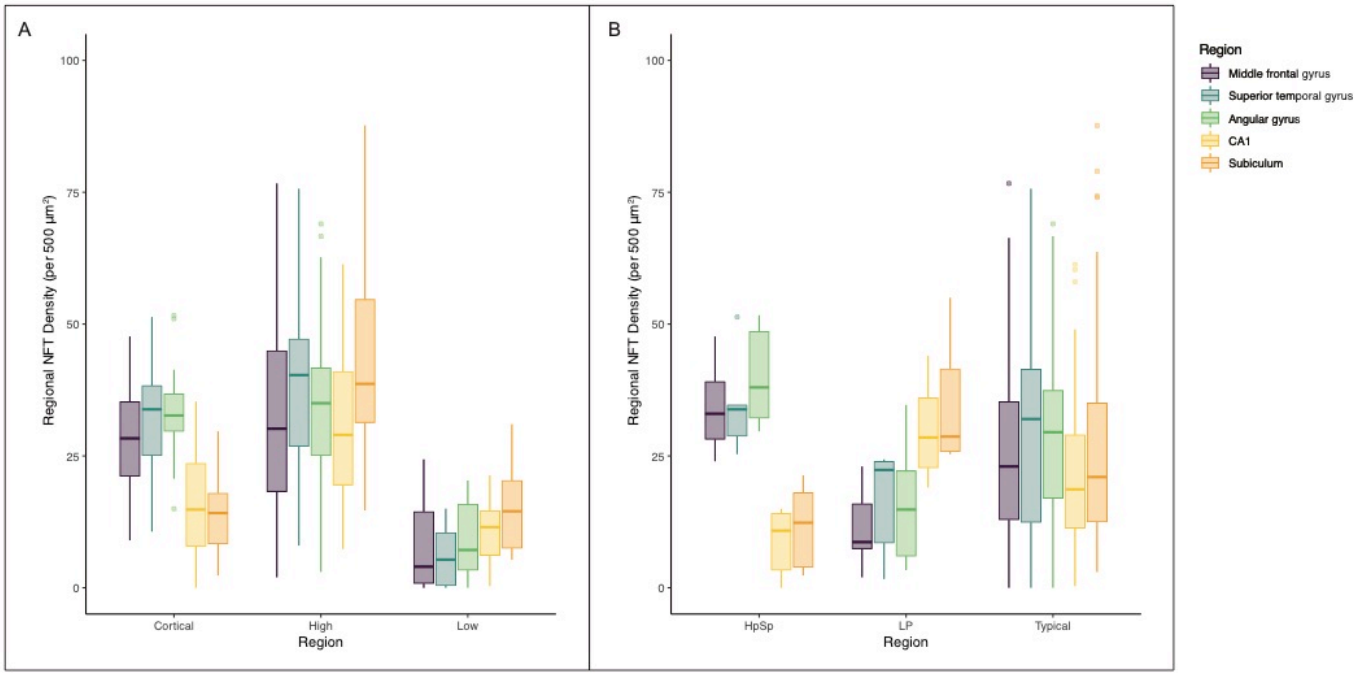

Table 3. Clinical and demographic characteristics according to NFT pathological clusters defined by Ward's hierarchical clustering and by manual algorithm. Differences between groups were assessed using Kruskal Wallis tests with post hoc pairwise Mann-Whitney U-test comparisons for continuous data. The false discovery rate (FDR) was set to <0.05. Differences for categorial data was assessed using Chi square tests.

a - Pairwise comparison of "cortical-predominant" cluster and "high overall" cluster, FDR-corrected $p < 0.05$

b - Pairwise comparison of "cortical-predominant" cluster and "low overall" cluster, FDR-corrected $p < 0.05$

c - Pairwise comparison of "low overall" cluster and "high overall" cluster, FDR-corrected $p < 0.05$

d - Pairwise comparison of typical AD subtype and HpSp AD subtype, FDR-corrected $p < 0.05$

	Ward's hierarchical clustering				Algorithmic subtypes			
Variable	Cortical-predominant	High overall	Low overall	*p value*	HpSp	LP	Typical	*p value*
n	24	30	18	-	6	6	60	-
Proportion male	0.63	0.33	0.89	*0.0007* [c]	0.50	0.67	0.57	*0.8389*
Proportion atypical clinical variant	0.39	0.55	0.46	*0.5817*	0.33	1.00	0.43	*0.0746*
Proportion APOE ε4 carriers	0.42	0.40	0.17	*0.1766*	0.50	0.17	0.35	*0.4764*
Mean age of onset (SD)	59.67 (8.38)	55.47 (7.75)	65.82 (9.34)	*0.0013* [b,c]	57.83 (6.15)	62.67 (10.69)	59.19 (9.36)	*0.5381*
Mean age of death (SD)	68.63 (9.18)	67.40 (8.90)	76.00 (10.17)	*0.0162* [b,c]	64.67 (6.65)	71.83 (11.02)	70.30 (9.97)	*0.2724*
Mean disease duration (SD)	8.96 (2.82)	11.93 (3.95)	10.12 (3.50)	*0.0301* [a]	6.83 (1.94)	9.17 (3.25)	11.00 (3.65)	*0.0102* [d]
Mean years of education (SD)	15.23 (3.29)	15.93 (2.27)	16.83 (3.31)	*0.3633*	15.00 (4.86)	16.00 (2.83)	16.04 (2.76)	*0.9948*
Mean CDR-SOB (SD)	7.31 (4.52)	11.18 (5.30)	8.92 (5.80)	*0.0480* [a]	8.33 (4.18)	8.25 (3.57)	9.47 (5.66)	*0.8051*
Mean executive z-score (SD)	-3.07 (1.09)	-3.57 (0.90)	-2.42 (1.66)	*0.0477*	-3.51 (0.80)	-2.29 (0.69)	-3.11 (1.33)	*0.1622*
Mean language z-score (SD)	-4.82 (3.06)	-4.61 (2.71)	-3.06 (1.67)	*0.1367*	-3.32 (1.97)	-2.85 (1.04)	-4.44 (2.77)	*0.2941*
Mean visuospatial z-score (SD)	-6.13 (3.55)	-6.34 (3.59)	-3.84 (3.74)	*0.0702*	-6.86 (2.96)	-4.78 (3.80)	-5.51 (3.81)	*0.6709*
Mean memory z-score (SD)	-3.90 (1.55)	-4.30 (1.42)	-3.44 (1.66)	*0.0984*	-4.09 (0.86)	-4.23 (1.12)	-3.90 (1.64)	*0.9509*

REFERENCES

1. Lam B, Masellis M, Freedman M, Stuss DT, Black SE. Clinical, imaging, and pathological heterogeneity of the Alzheimer's disease syndrome. Alzheimers Res Ther. 2013;5(1):1.

2. Coughlin D, Xie S, Liang M, et al. Cognitive and Pathological Influences of Tau Pathology in Lewy Body Disorders. Ann Neurol. 2019;85: 259-271.

3. Murray ME, Graff-Radford NR, Ross OA, Petersen RC, Duara R, Dickson DW. Neuropathologically defined subtypes of Alzheimer's disease with distinct clinical characteristics: A retrospective study. Lancet neurology. 2011;10(9):785-796.

4. Jadhav S, Cubinkova V, Zimova I, et al. Tau-mediated synaptic damage in Alzheimer's disease. Transl Neurosci. 2015;6(1):214-226.

5. Suemoto CK, Ferretti-Rebustini RE, Rodriguez RD, et al. Neuropathological diagnoses and clinical correlates in older adults in Brazil: A cross-sectional study. PLoS Med. 2017;14:e1002267.

6. Braak H, Braak E. Neuropathological stageing of Alzheimer-related changes. Acta Neuropathol 1991;82:239–259.

7. Janocko NJ, Brodersen KA, Soto-Ortolaza AI, et al. Neuropathologically defined subtypes of Alzheimer's disease differ significantly from neurofibrillary tangle-predominant dementia. Acta neuropathologica. 2012;124(5):681-692.

8. Ossenkoppele R, Schonhaut DR, Schöll M, et al. Tau PET patterns mirror clinical and neuroanatomical variability in Alzheimer's disease. Brain. 2016;139(Pt 5):1551-67.

9. Hauw JJ, Daniel SE, Dickson D, et al. Preliminary NINDS neuropathologic criteria for Steele-Richardson-Olszewski syndrome (progressive supranuclear palsy). Neurology. 1994;44: 2015-2019.

10. Dickson DW, Bergeron C, Chin SS, et al. Office of Rare Diseases neuropathologic criteria for corticobasal degeneration. J Neuropathol Exp Neurol. 2002;61: 935-946.

11. McKeith IG, Dickson DW, Lowe J, et al. Diagnosis and management of dementia with Lewy bodies: third report of the DLB Consortium. Neurology. 2005;65: 1863-1872.

12. Cairns NJ, Bigio EH, Mackenzie IR, et al. Neuropathologic diagnostic and nosologic criteria for frontotemporal lobar degeneration: consensus of the Consortium for Frontotemporal Lobar Degeneration. Acta Neuropathol. 2007;114: 5-22.

13. Montine TJ, Phelps CH, Beach TG, et al. National Institute on Aging-Alzheimer's Association guidelines for the neuropathologic assessment of Alzheimer's disease: a practical approach. Acta Neuropathol. 2012;123: 1-11.

14. Mackenzie IR, Neumann M, Bigio E, et al. Nomenclature and nosology for neuropathologic subtypes of frontotemporal lobar degeneration: an update. Acta Neuropathol 2010;119: 1-4.

15. Mackenzie IR, Neumann M, Baborie A, et al. A harmonized classification system for FTLD-TDP pathology. Acta Neuropathol. 2011;122: 111-113.

16. Kovacs GG, Ferrer I, Grinberg LT, et al. Aging-related tau astrogliopathy (ARTAG): harmonized evaluation strategy. Acta Neuropathol. 2016;131(1):87-102.

17. McKhann GM, Drachman D, Folstein M, Katzman R, Price D, Stadlan EM. Clinical diagnosis of Alzheimer's disease: report of the NINCDS-ADRDA Work Group under the auspices of Department of Health and Human Services Task Force on Alzheimer's Disease. Neurology. 1984;34: 939-944

18. McKhann GM, Knopman DS, Chertkow H, et al. The diagnosis of dementia due to Alzheimer's disease: recommendations from the National Institute on Aging-Alzheimer's Association workgroups on diagnostic guidelines for Alzheimer's disease. Alzheimers Dement. 2011;7: 263-269.

19. Dubois B, Feldman HH, Jacova C, et al. Advancing research diagnostic criteria for Alzheimer’s disease: the IWG-2 criteria. Lancet Neurol. 2014; 13: 614-629.

20. Armstrong MJ, Litvan I, Lang AE, et al. Criteria for the diagnosis of corticobasal degeneration. Neurology. 2013;80: 496-503.

21. Gorno-Tempini ML, Hillis AE, Weintraub S, et al. Classification of primary progressive aphasia and its variants. Neurology. 2011;76: 1006-1014.

22. Crutch SJ, Lehmann M, Schott JM, Rabinovici GD, Rossor MN, Fox NC. Posterior cortical atrophy. Lancet Neurol. 2012; 11: 170-178.

23. Crutch SJ, Schott JM, Rabinovici GD, et al. Consensus classification of posterior cortical atrophy. Alzheimers Dement. 2017;13: 870-884.

24. Neary D, Snowden JS, Gustafson L, et al. Frontotemporal lobar degeneration: a consensus on clinical diagnostic criteria. Neurology. 1998;51: 1546-1554.

25. Rascovsky K, Hodges JR, Knopman D, et al. Sensitivity of revised diagnostic criteria for the behavioural variant of frontotemporal dementia. Brain. 2011;134: 2456-2477.

26. Petersen RC, Smith GE, Waring SC, Ivnik RJ, Tangalos EG, Kokmen E. Mild cognitive impairment: clinical characterization and outcome. Arch Neurol. 1999;56: 303-308

27. Albert MS, Dekosky ST, Dickson D, et al. The diagnosis of mild cognitive impairment due to Alzheimer's disease: Recommendations from the National Institute on Aging-Alzheimer's Association workgroups on diagnostic guidelines for Alzheimer's disease. Alzheimers Dement. 2011;7: 270-279.

28. Kaplan E, Goodglass H, Weintraub S. Boston naming test. Philadelphia: Lea & Febiger, 1983.

29. Dunn LM, Dunn DM; Pearson A. PPVT-4 : Peabody picture vocabulary test. Minneapolis: Pearson Assessments, 2007.

30. Knopman DS, Kramer JH, Boeve BF, et al. Development of methodology for conducting clinical trials in frontotemporal lobar degeneration. Brain. 2008;131(11):2957-2968.

31. Staffaroni AM, Brown JA, Casaletto KB, et al. The Longitudinal Trajectory of Default Mode Network Connectivity in Healthy Older Adults Varies As a Function of Age and Is Associated with Changes in Episodic Memory and Processing Speed. J Neurosci. 2018;38(11):2809-2817.

32. Terry RD, Hansen LA, Deteresa R, Davies P, Tobias H, Katzman R. Senile Dementia of the Alzheimer Type Without Neocortical Neurofibrillary Tangles. Journal of Neuropathology and Experimental Neurology. 1987;46(3):262-268.

33. Kaiser HF. The Application of Electronic Computers to Factor Analysis. Educational and Psychological Measurement, 1960;20(1), 141–151.

34. Cattell RB. The Scree Test for the Number of Factors. Multivariate Behavioral Research. 1966;1(2):245–76.

35. Szekely G, Rizzo M. Hierarchical Clustering via Joint Between-Within Distances: Extending Ward's Minimum Variance Method. Journal of Classification. 2005;22: 151.

36. Brock G, Pihur V, Datta S, et al. clValid: An R Package for Cluster Validation. Journal of Statistical Software. 2008;25(4): 1-22.

37. Kaufman L, Rousseeuw PJ. Finding groups in data: An introduction to cluster analysis. John Wiley & Sons, New York, 2005.

38. Savva GM, Wharton SB, Ince PG, Forster G, Matthews FE, Brayne C. Age, neuropathology, and dementia. The New England Journal of Medicine. 2009;360(22):2302-9.

39. Ohm TG, Scharnagl H, März W, Bohl J. Apolipoprotein E isoforms and the development of low and high Braak stages of Alzheimers disease-related lesions. Acta Neuropathologica. 1999;98(3):273-280.

40. Xia C, Makaretz SJ, Caso C, et al. Association of In Vivo [18F]AV-1451 Tau PET Imaging Results With Cortical Atrophy and Symptoms in Typical and Atypical Alzheimer Disease. JAMA Neurol. 2017;74(4):427-436.

41. Seghier ML. The Angular Gyrus: Multiple Functions and Multiple Subdivisions. The Neuroscientist. 2013;19(1):43-61.

42. Ji J, Maren S. Differential roles for hippocampal areas CA1 and CA3 in the contextual encoding and retrieval of extinguished fear. Learning & Memory. 2008;15(4):244-251.

43. Leutgeb S, Leutgeb JK, Barnes CA, Moser EI, McNaughton BL, Moser MB. Independent codes for spatial andepisodic memory in hippocampal neuronal ensembles. Science. 2005;309:619–623.

44. Giannakopoulos P, Herrmann FR, Bussiere T, et al. Tangle and neuron numbers, but not amyloid load, predict cognitive status in Alzheimer's disease. Neurology. 2003;60(9):1495-1500.

45. Gomez-Isla T, Hollister R, West H, et al. Neuronal loss correlates with but exceeds neurofibrillary tangles in Alzheimer's disease. Ann Neurol. 1997;41(1):17-24.

46. La Joie R, Visani A, Bourakova V. AV1451-PET cortical uptake and regional distribution predicts longitudinal atrophy in Alzheimer’s disease. Alzheimer's & Dementia. 2017;13(7):904.

47. Everitt BS. Unresolved Problems in Cluster Analysis. Biometrics. 1979;35(1):169.